Advanced Powder Technology 23 (2012) 485–492

Contents lists available at SciVerse ScienceDirect

Advanced Powder Technology

journal homepage: www.elsevier.com/locate/apt

Original Research Paper

Numerical solution of gas–solid flow in fluidised bed at sub-atmospheric pressures

Apurv Kumar *, Peter Hodgson, Daniel Fabijanic, Weimin Gao

Institute for Frontier Materials, ITRI, Deakin University, Geelong 3216, Australia

ARTICLE INFO

Article history:
Received 29 December 2011
Received in revised form 12 April 2012
Accepted 22 April 2012
Available online 8 May 2012

Keywords:
Gas–solid fluidisation
CFD
Drag model
Vacuum fluidisation

ABSTRACT

Fluidised beds are characterised by excellent thermal and chemical uniformity and have a wide application range including heat and surface treatment, ore roasting and catalyst production. However, compared to other gas-based systems, to fluidise a particulate mass, a significant quantity of gas is required. To conserve gas there is potential to operate the fluid bed under low-pressure conditions. It is also observed that heat transfer remains constant with reduction in pressure. The present work has numerically studied the nature of hydrodynamics in fluidised bed at sub-atmospheric conditions and a new drag law is proposed to account for the increased mean free path of the fluid. A wide range of sub-atmospheric pressures were considered such that slip flow regime, which is characterised with $Kn \sim 1$, is applicable. An open source code (MFIX) is used to numerically solve the multiphase problem of a jet in the fluidised bed column with an immersed surface at vacuum pressure conditions. Bubbling fluidisation in shallow and deep beds are also solved. The new drag model takes into consideration the effect of slip flow to model drag force on the particles and the results of velocity distributions in the column and around the submerged surface is presented. The results of velocity distributions from the slip flow model are compared with the existing Gidaspow's model. Significant differences were observed in the simulation results of velocity distributions and flow structure in the fluidised bed under vacuum conditions.

1. Introduction

Fluidisation is the achieving of a fluid like behaviour for any solid granular entities with the help of a fluidising media, such as gasses and liquids. The fluidising medium displaces and suspends the solid granular particles from their static position, transferring the momentum and resulting in fluid like motion of the particles. These particles being fluid borne are free to move from one location to another in a seemingly random manner. It is this random motion of the particles that resembles the flow of a fluid and hence the name fluidisation. It is a commonly used phenomenon in chemical industries and is used in processes such as mineral cracking, heat treatment, surface engineering etc. Fluidisations phenomenon offers a processing environment with a wide spectrum of advantages. The ability to achieve uniformity of temperature, high solid–fluid mixing leading to high heat and mass transfer and continuous operation, make the use of fluidisation quite appealing.

To understand the complex multiphase flow behaviour inside gas–solid fluidised beds the mathematical models proposed mainly fall under four groups depending on how they treat each phase and the magnitude of the length scales. These are (1) Discrete Bubble model, (2) Two-fluid model, (3) Discrete Particle model and (4) Molecular Dynamics model. In other words, each of these models considers the gas–solid phases to be either Eulerian or Lagrangian [1]. Selection of these models depends mostly on the geometry to be modelled and the available computing resources. Of these, most popular are the Two-fluid models where the two phases are modelled as interpenetrating continua. Each of the two phases are modelled as separate fluid (gas and solid) and is solved by Eulerian method (classical Navier–Stokes equation). The solid–fluid coupling is given by drag force that appears in the momentum balance equation for each phase and is equal in magnitude but opposite in direction.

Operation of fluidised bed at various pressure ranges (sub-atmospheric to high pressures) offers advantages that make the use of fluidised bed reactors (FBR) even more appealing. In the literature, fluidised beds at high pressures have been studied extensively. A comprehensive review is given by Yates [2] on the effect of pressure and temperature on gas–solid fluidisation. Coal combustion and gasification are the primary areas of interest for high-pressure fluidisation. Although, high pressures greatly effects heat and mass transfer rates, certain heat sensitive materials such as thermolabile substances, used in pharmaceutical industry for coating and drying purposes, cannot be used at high pressures.

* Corresponding author. Address: Waurn Ponds Campus, Deakin University, GTP Building, Room No. na.1.2300, Geelong 3216, Australia. Tel.: +61 (03) 52273360.
E-mail address: apurv@deakin.edu.au (A. Kumar).

0921-8831/$ - see front matter © 2012 The Society of Powder Technology Japan. Published by Elsevier B.V. and The Society of Powder Technology Japan. All rights reserved.
http://dx.doi.org/10.1016/j.apt.2012.04.010

Nomenclature

Notations

d	diameter , m
D	width of the fluidising column, m (=0.57 m)
e	restitution coefficient
F	momentum exchange coefficient, Pa s/m^2
g	acceleration due to gravity, m/s^2
k	diffusion coefficient
K	Boltzmann's constant , J/K (=1.3806x10^{-23})
Kn	Knudsen number (λ/d)
L	bed height, m
P	pressure, N/m^2
Re	Reynolds number, ρ_f Vd$_p$/μ
T	temperature, K
u	superficial velocity, m/s
y	length along y-direction
v	velocity vector, m/s

Greek letters

ε	void fraction
ψ	interstitial angle
ϕ	sphericity
μ	dynamic viscosity, Pa s
ξ	molecular diameter of gas, m (=3.7 $\times$ 10^{-7} m)
ρ	density, kg/m^3
λ	mean free path of gas, m

Subscripts

g	gas
mf	minimum fluidisation
s	solid

An alternative is to use sub-atmospheric pressure conditions as it reduces the possibility of partial degradation of thermolabile substances and the process is made safer by operating outside the flammability ranges. Bhat and Whitehead [3] carried out experiments to study the effect of sub-atmospheric pressures on heat transfer from an immersed surface in fluidised bed reactors. Cooling water tubes were passed across the fluidised bed and the overall heat transfer coefficient was determined for various operating pressures and superficial velocity. At constant superficial velocity, the heat transfer coefficient remained constant with decrease of pressure, thus establishing the advantage of low-pressure fluidisation.

Suezawa and Kawamura [4] were the first to study the mechanism of fluid flow in fluidised bed at reduced pressures. It was observed from the fluidisation of sand, silica gel and glass beads (at pressures 0.133–13.33 kPa) that the behaviour of fluidised bed at reduced pressure resembled the bed at atmospheric pressure. In experiments (pressure range of 0.533–4 kPa) by Germain and Claudel [5] a coexistence of upper fluidised layer and a bottom quiescent layer was observed for deep beds. Llop et al. [6] gave an expression for minimum fluidisation velocity which accounts for the operating pressures. This expression predicted the minimum fluidisation velocity in vacuum conditions as well as higher pressures accurately. Expression for minimum fluidisation velocity at atmospheric pressures given by Wen and Yu [7] and Ergun [8] were compared with Llop's equation and a significant difference in prediction of the velocity with change in pressure at vacuum conditions was found. Llop's equation accounts for the increase of mean free path of the fluid particles and its effect on the pressure drop in the bed and hence deals with the physics of fluidisation more comprehensively. However, this equation does not accurately predict the minimum fluidisation velocity for fine particles. Wank et al. [9] accounted for the inter-particle cohesive forces in Llop's equation which predicted the minimum fluidisation velocity of fine boron nitride powders accurately. Thus, most of the work done in low pressure fluidised beds found in literature deals mainly with basic experimental and theoretical study of hydrodynamics of fluidised bed. There has been no work reported in literature that numerically simulates and studies the hydrodynamics of low-pressure fluidised bed. Therefore, the scope of the present work is to numerically solve the hydrodynamics of a gas–solid fluidised bed at sub-atmospheric pressures using the Two-fluid model by incorporating the effect of slip flow and compare it with the widely used drag model of Gidaspow [10]. Two cases of gas–solid fluidisation are modelled: *case* (*a*) fluidised bed with an immersed surface and *case* (*b*) bubbling fluidisation in shallow and deep beds. The numerical solution to the two-phase model is carried out by an open source code, MFIX.

2. Two-fluid model and drag laws

Two-fluid model considers each of the phase to be interpenetrating continua and the governing equations of mass and momentum conservations are solved for each of the phases which are local mean averages of the point fluid and particles variables. Descriptions of the mass and momentum governing equations are presented extensively in MFIX theory guide [11] and in the Supplementary section.

For the problem to be completely defined the governing equations requires closures for the solid-phase pressure (P_s), solid-phase shear viscosity (μ_s) and the solid-phase bulk viscosity (λ_s). These constitutive equations are derived from kinetic theory of granular flow and are presented in Table 1 of the Supplementary information section. Apart from these closures, kinetic theory of granular flow requires the solution to transport equation for the granular temperature. Granular temperature, Θ, signifies the random motion of the solid particles and is analogous to temperature definition according to the Kinetic theory [12]. In order to account for the friction between the solid particles when the void fraction in the bed approaches the packing limit, a frictional stress model

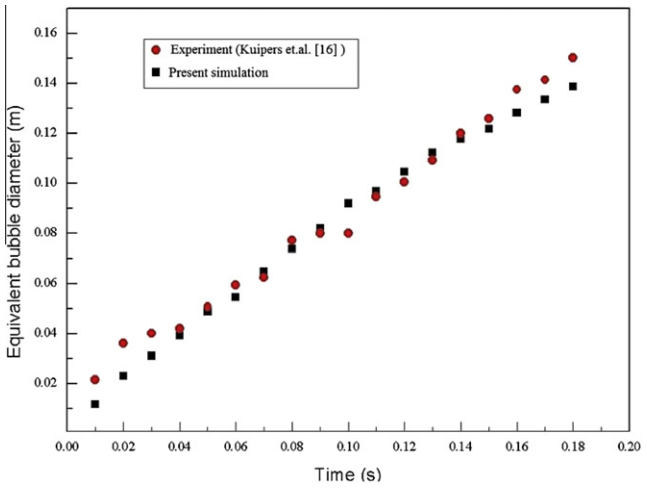

Fig. 1. Comparison of simulated equivalent bubble diameter in the fluidised bed with Kuipers [16] experiment.

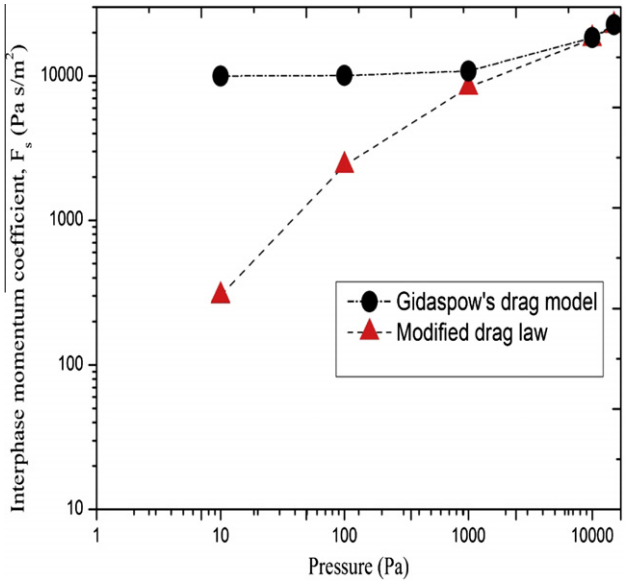

Fig. 2. Comparison of Gidaspow's drag law and the modified drag law for prediction of F_s with decrease of pressure.

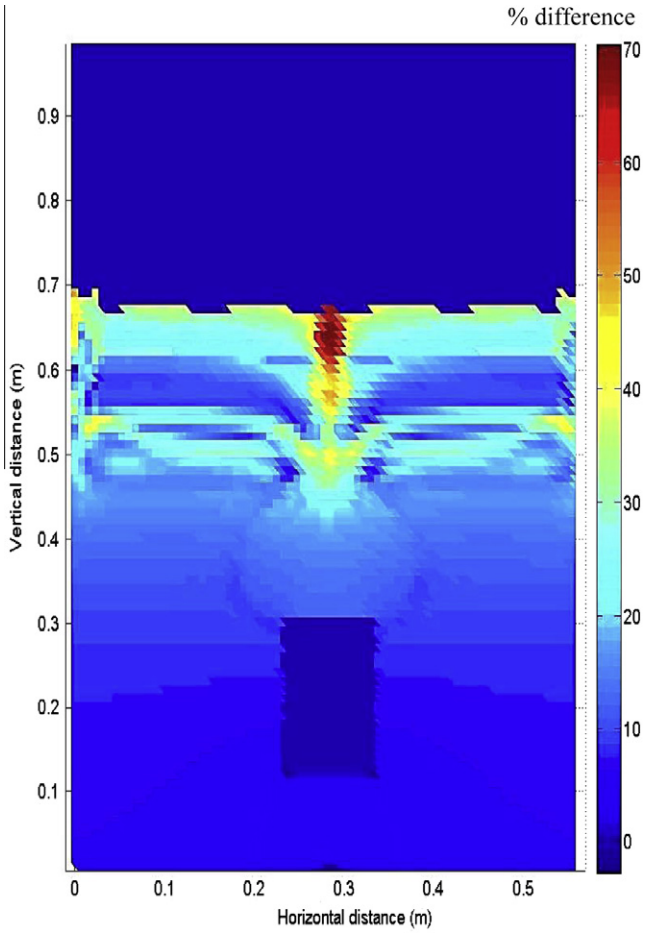

Fig. 3. Percentage difference in time averaged value of F_s between Gidaspow's model and the modified drag model in the fluidised bed at 100 Pa.

that forms a part of the solid shear stress tensor is generally used. In the present work, the frictional stress model of and Srivastava and Sunderasan [13] is used, which has been shown in literature

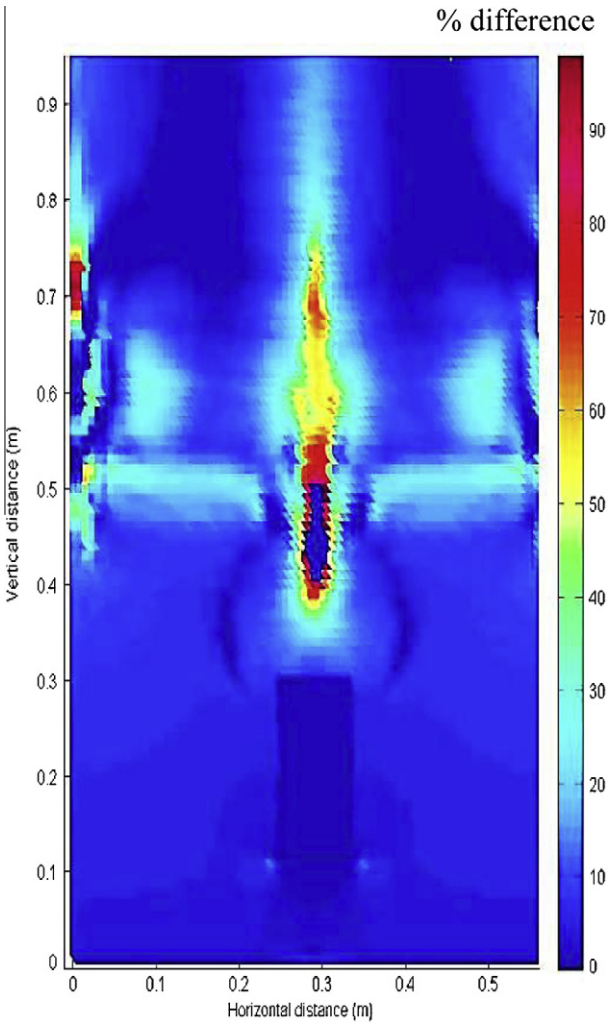

Fig. 4. Percentage difference in time averaged velocity between Gidaspow's model and the modified drag model for the immersed surface case at 100 Pa.

to accurately predict the shape and size of a bubble in fluidised bed [14].

Coupling between the solid and fluid phase in Two-fluid model is through the interphase momentum exchange coefficient, F_s. Several semi-empirical closures exist in literature to define F_s. Of these, the Gidaspow's model [10] is the widely used drag law and is a combination of drag law by Ergun [8] and Wen and Yu [7].

In vacuum conditions, as the pressures are reduced below atmospheric, the mean free path of the fluid particles increases. This is characterised by Knudsen number, which is the ratio of mean free path ($\lambda = \frac{KT}{\sqrt{2}\pi\zeta^2 p}$) to a length scale, d. Knudsen number increases with decreasing pressures that changes the nature of the fluid flow. Molecular flow (Kn >> 1), intermediate or slip flow (Kn $\sim$ 1) and laminar flow (Kn << 1) are found to exist in vacuum conditions. Llop et al. [6] derived pressure drop equations for flow through fluidised bed and predicted the minimum fluidisation velocity (u_{mf}) by considering slip flow regime [7]. In the present work, the Gidaspow's drag law is modified to include the effect of slip flow regime by incorporating the effect of Kn on fluid flow and its effect on gas–solid fluidisation is studied.

2.1. Modified drag law

The pressure drop equation through a fluidised bed which accounts for operating pressures is given by Llop et al. [6].

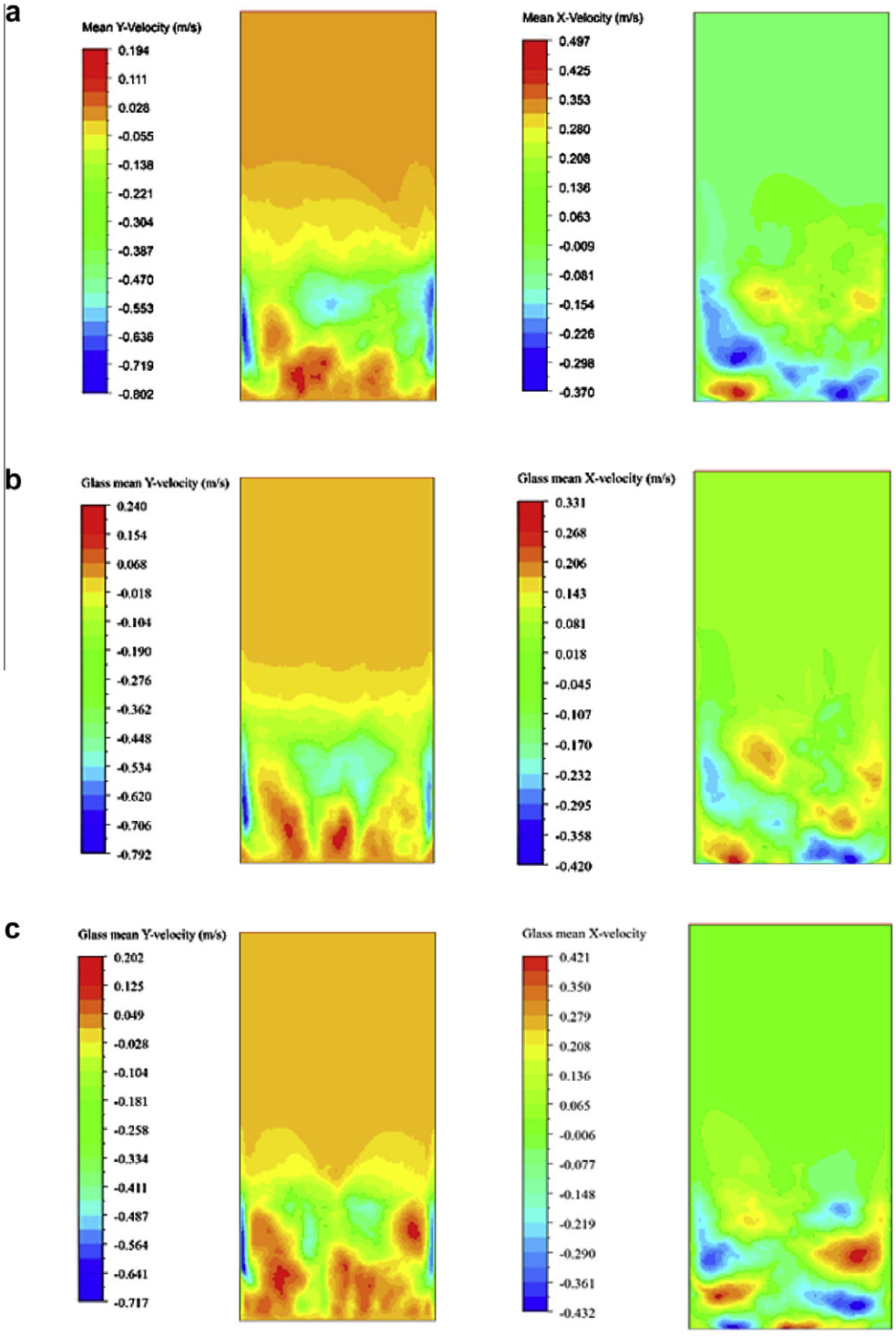

Fig. 5. Contours of time averaged velocity for shallow beds predicted by the drag models. (a) Modified drag law at 1000 Pa (b) Gidaspow drag model at 1000 Pa (c) Gidaspow drag model at atmospheric pressure.

$$\frac{dp}{dl} = \frac{u}{\frac{16}{45}\cos^2\psi\,\frac{\varepsilon_g^2\phi d_s}{(1-\varepsilon_g)}\sqrt{\frac{2}{\pi\rho P}} + \frac{\cos^2\psi}{72}\,\frac{\varepsilon_g^3(\phi d_s)^2}{\mu_g(1-\varepsilon_g)^2}} + 1.75\frac{(1-\varepsilon_g)}{\varepsilon_g^3\phi d_s}\rho u^2 \qquad (1)$$

This can be extended to derive the interphase momentum coefficient, F_s since the pressure drop in a fluidised bed can also be expressed as [10]:

$$\frac{dp}{dl} = \frac{F_s}{\varepsilon_g}(\vec{v}_g - \vec{v}_s) \qquad (2)$$

This upon comparison with Eq. (1) and substituting the constants given by Llop et al. [6] yields the following expression for F_s, the inter phase momentum exchange coefficient:

$$F_s = \frac{(1-\varepsilon_g)}{0.1356\phi d_s\sqrt{\frac{1}{\rho P}} + \frac{1}{150}\,\frac{\alpha_g}{(1-\varepsilon_g)\mu_g}(\phi d_s)^2} + 1.75\frac{\rho_g(1-\varepsilon_g)(\vec{v}_g - \vec{v}_s)}{\phi d_s} \qquad (3)$$

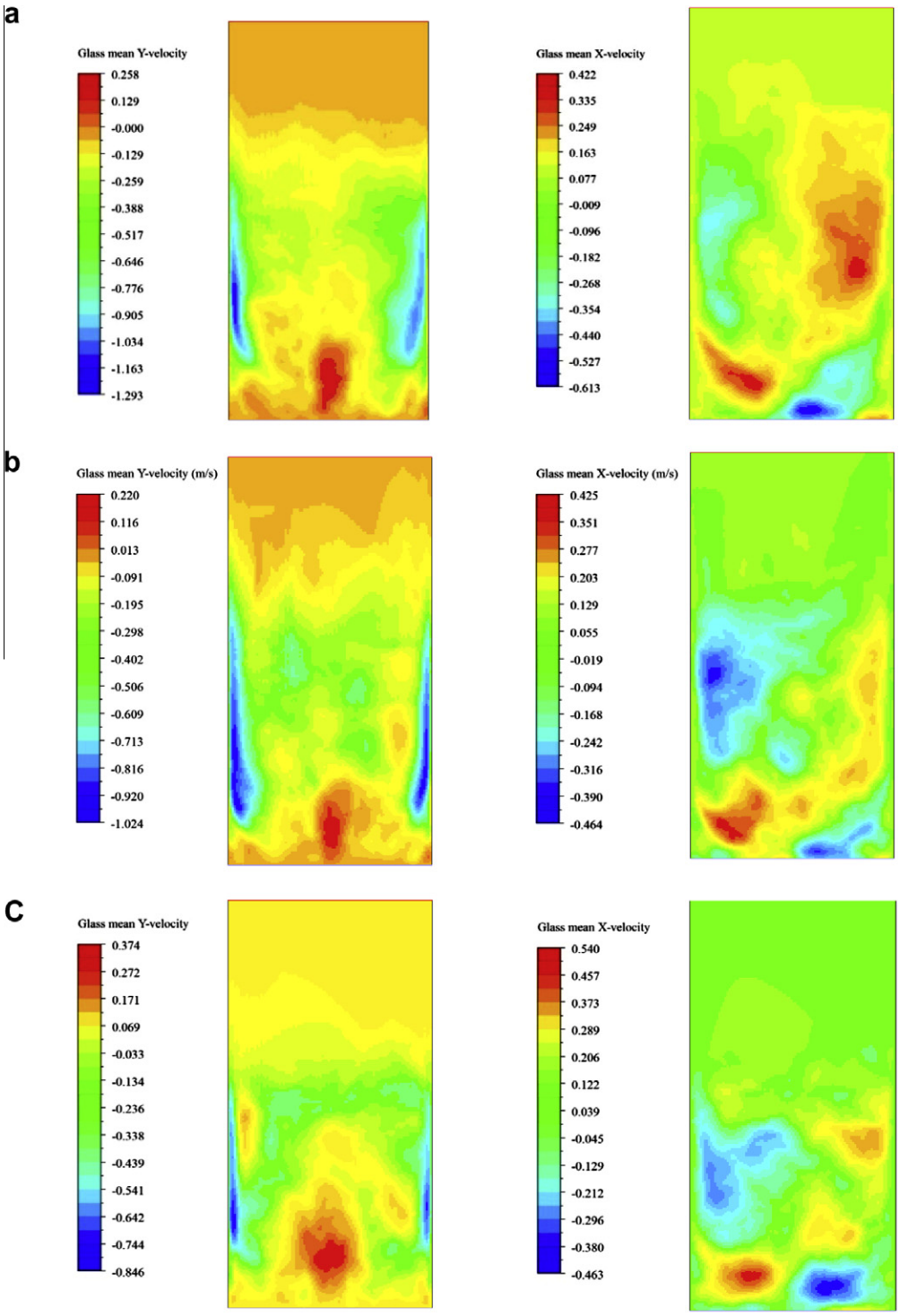

Fig. 6. Contours of time averaged velocity for deep beds predicted by the drag models. (a) Modified drag law at 1000 Pa (b) Gidaspow drag model at 1000 Pa (c) Gidaspow drag model at atmospheric pressure.

Eq. (3) accommodates the effect of slip flow and is equal to the Ergun's equation [8] in the limit $P \to \infty$.

3. Problem description and numerical simulations

The sub-atmospheric pressure conditions in a fluidised bed, where slip flow is predominant, were solved numerically using the modified drag law (Eq. (3)) derived in earlier section. Different cases are studied under vacuum conditions which includes a two dimensional rectangular column of size 0.57 × 1 m with a central jet (0.015 m) and an immersed rectangular surface (0.1×0.2 m). Apart from this, a fluid bed of same dimension without the immersed surface but with varying aspect ratio of the bed was solved additionally in the present numerical study. Glass beads of size 500 μm were used in the simulation. Simulations were carried out by an open source code (MFIX) and the initial and boundary conditions for the bed with immersed surface are given in the Supplementary information section. For the case where immersed

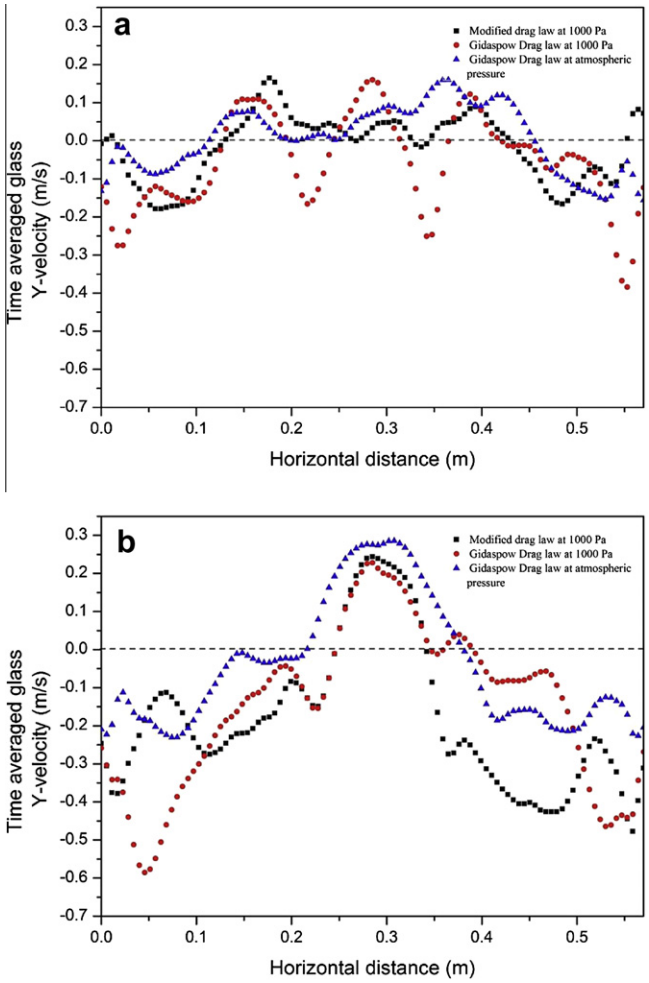

Fig. 7. Time averaged velocity profiles at an axial location as predicted by the drag models in the bubbling fluidised bed. (a) Shallow beds at $y = 0.05$m (b) deep beds at $y = 0.1$m

surface and the jet were absent, a uniform inlet velocity of $1.5U_{mf}$ was applied in order to simulate bubbling fluidisation. A uniform velocity of $1.5\varepsilon_{mf}U_{mf}$ in the bed and $1.5U_{mf}$ in the freeboard region was specified as initial conditions for bubbling fluidisation model. A uniform grid of size 0.01 m was considered along the length of the column and 0.0075 m was considered along the width of the bed for the model of immersed surface. A grid independent study revealed that fine mesh was successful in simulating meso-scale structures for the case of fluid beds without the immersed surface. Due to limitation of computational resources, a non-uniform grid size of 10^{-3} along the width and 0.01 along the length of the fluid bed was selected with finer mesh in the bed region. The Gidaspow's drag law was modified by replacing the interphase momentum coefficient by Eq. (3) for dense regions in the bed. A time step of 10^{-4} s was used in all simulations and a residual limit of 10^{-4} for continuity, momentum and granular temperature terms was used.

No slip wall-boundary conditions was used for the gas-phase whereas partial slip wall-boundary condition given by Johnson and Jackson [15] was applied to solid-phase with specularity coefficient as 0.5 and particle–wall coefficient of restitution (e) as 0.9.

4. Results and discussion

In order to validate the numerical model, the fluidised bed is operated with a jet of higher velocity ($40U_{mf}$). The bed is operated at ambient pressure conditions and the Gidaspow's drag model is used. The equivalent bubble diameter is compared with the experimental results of Kuipers [16]. The equivalent bubble diameter is defined as the diameter of the circle enclosed by $\varepsilon_g \geqslant 0.8$. Fig. 1 shows the comparison of the diameter with the experiments and it can be seen that the numerical model accurately predicts the diameter up to the detachment point of 0.2 s. This is consistent with other results found in literature [14]. In addition to observing the residuals, the gas-mass flow conservation through the inlet and outlet boundary is also calculated for each simulation and the average error reported was ±5% for each time step.

The modified drag law (Eq. (3)) is compared with the Gidaspow's drag model for values of the terms appearing in the equation in order to examine the prediction of F_s with reduction in pressure. Fig. 2 shows the variation of F_s with pressure and it can be seen that there is significant difference between the modified drag law and that of Gidaspow's, both in terms of magnitude and trend at high vacuum conditions. The linear variation of F_s with pressure for Gidaspow's model is due to change in density of the fluid with pressure. This model does not account for the effects of slip flow, which becomes predominant at high vacuum pressures. Llop et al. [6] has shown that slip flow regime influences the prediction of minimum fluidisation velocity which is derived by balancing the total drag force to the weight of the bed. Interestingly, the models of Wen and Yu were not able to capture this effect [6], thus showing that the drag forces predicted by them were inaccurate in vacuum conditions.

The operating pressure was reduced to high vacuum pressures (1000–100 Pa) in order to study the effect of the operating pressure on prediction of F_s. As can be seen from Fig. 2, the existing Gidaspow's model over-predicts the magnitude of F_s at high vacuum pressures and the modified drag law starts to deviate at pressures in the range 1000 Pa. The pressure drop through the bed reduces with increase of mean free path of the fluid. As a result, the fluid does not effectively transport the momentum to the solid particles and retains the momentum while passing through the bed. Therefore, a higher velocity is required for the drag force to balance the weight of the bed or to displace the particles upwards.

4.1. Case (a): Immersed surface with central jet

A number of simulations were run in order to compare the effect of the bubble size and its movement through the bed predicted by the modified drag law with those predicted by the Gidaspow's model. The first term in the denominator of F_s (Eq. (3)) becomes comparable to the second term only at high vacuum pressures. It is seen that this occurred at a pressure of 1000 Pa for the present set of conditions. Since a linear pressure gradient exists in the bed, which is tantamount to the bed weight, the magnitude of F_s as predicted by the modified drag law was significantly lower than the Gidaspow's model especially at the top of the bed.

Fig. 3 shows the percentage difference in the time-averaged values of F_s as predicted by the Gidaspow's model and the modified model for operating pressure at 100 Pa. All time average results are for a period of 3 s. As seen from the contour plot, a maximum difference of 70% and an average difference of 18% in the bed region exist between Gidaspow's model and the modified model, with the Gidaspow's model predicting a higher value. In addition, the difference increases linearly and the maximum occurs near the interface of bed and the freeboard region. The modified slip-flow drag law also predicted a lower bed height.

Due to lower values of F_s predicted by the modified drag law, the velocity of air was found to be greater than those predicted by the Gidaspow's model especially towards the top of the bed which can be seen in Fig. 4. This is due to the inefficiency of the air to transfer momentum to the solid particles. Consequently, the velocity of solid particles in the bed was found to be lower in

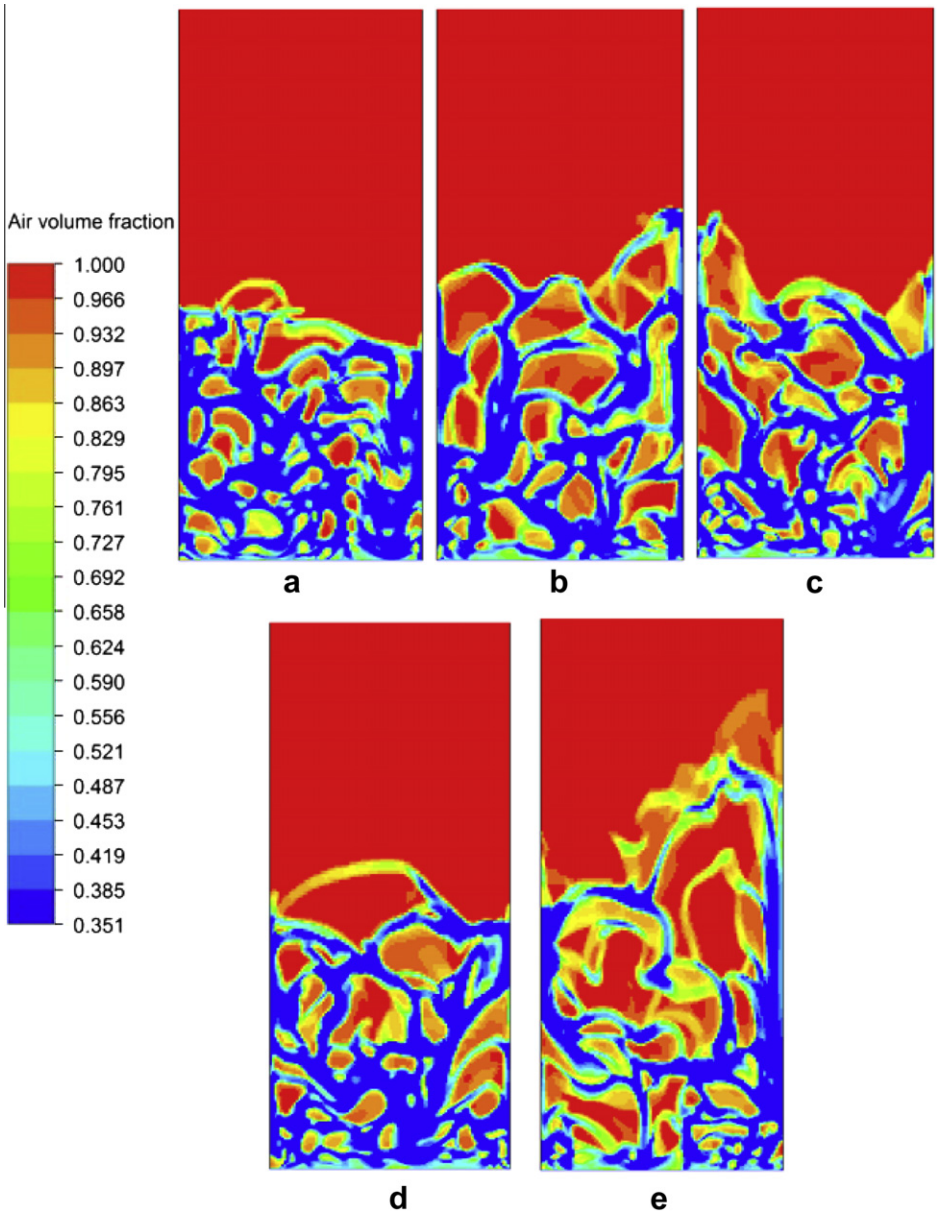

Fig. 8. Volume fraction of air for deep beds at 3 s for $1.5U_{mf}$. (a) Atmospheric conditions (b) at 10^4 Pa using modified drag law (c) at 10^4 using Gidaspow drag model (d) at 10^3 Pa using modified drag law (e) at 10^3 Pa using Gidaspow drag model.

the simulations where the modified drag law was used. The bubble size at the bottom of the bed was of similar size and shape when the modified drag law was used in simulations. This is because the pressures at the bottom of the bed were of equal order of magnitude (around 8800 Pa) and therefore the predictions of velocity and F_s were of same order of magnitude at the bottom of the bed.

4.2. Case (b): Bubbling fluidisation in shallow and deep beds

Two cases of bubbling fluidisation with different aspect ratio (AR = L/D) were numerically solved: shallow (AR = 0.5) and deep beds (AR = 1). Bubble flow profile under vacuum conditions was observed in each of the simulations. Figs. 5 and 6 shows the time averaged x and y velocity contour plots (for a period of 3 s) for shallow beds and deep beds at atmospheric and sub-atmospheric conditions as predicted by the modified and Gidaspow's drag model. It is seen that the general flow profile of the emulsion phase is preserved with decrease of pressure – the emulsion phase rises in the core and descends at the walls. This nature of hydrodynamics is typical of fluidised beds [17]. In addition, the emulsion phase was seen to ascend uniformly in the bed region near the distributor at atmospheric pressure. The modified drag model predicts a similar profile whereas the Gidaspow's drag model predicts a profile that is concentrated in the middle of the bed (Fig. 5b).

The circulation pattern of emulsion phase can be determined by observing together the x and y velocity profiles (Figs. 5 and 6). In the shallow beds (Fig. 5), the circulation pattern reverses at vacuum pressures and the emulsion phase moves towards the core near the distributor plate while rising upwards whereas the emulsion phase moves towards the wall at atmospheric pressures in the same region. However, for the deep beds no such reversals in flow structure were seen with decrease of pressure. It can also be observed that for deep beds, both the drag models predict a different circulation pattern as compared to atmospheric conditions. As seen from Fig. 5 (a and b), the positive and negative velocity (the red and the blue region) are one above the other instead of being opposite, as seen in all other cases (shallow and atmospheric deep beds). It is seen in the case of the deep beds in vacuum pressure that a larger

region of maximum velocity of descent (region with blue colour in Fig. 6) of the emulsion phase near the walls was predicted by the Gidaspow's drag model. In all the simulation at vacuum pressures, an average difference of 20% is observed in prediction of the maximum emulsion phase rise velocity near the distributor plate by the two drag models. This result is consistent with those obtained from the case of an immersed surface in the fluidised bed.

Fig. 7 shows the velocity profiles at $y = 0.05$ m in the shallow bed and at $y = 0.1$ m in deep beds. It can be seen that the prediction of velocity profiles by the drag models at atmospheric and vacuum pressures are similar for deep beds. However, for the shallow bed the Gidaspow's drag model does not predict a uniform velocity profile whereas the modified drag model predicts a profile similar to the atmospheric conditions.

The volume fraction of air at different pressures (10^3, 10^4 and 101,325 Pa) and in deep bed (aspect ratio, AR = 1) is shown in Fig. 8 which are predicted by modified and the Gidaspow's drag model at the end of simulation at 3 s. Bubble size is seen to increase with reduction in pressure for both deep and shallow beds. This trend is opposite to what is observed in high-pressure fluidisation where the bubble size reduces with rise of pressure above atmospheric [2]. Gidaspow's model and the modified model both predicted this trend. It was seen at 10^3 Pa that the Gidaspow's model predicted larger bubble size and the bed seemed to slug at this pressure. This was not the case with the prediction from the modified drag law. There were no differences seen in prediction at 10^4 Pa from both the models. This is due to the fact that slip flow regime for 500 μm particles begin only at 6000 Pa (Kn = 0.01). The bubble size increase was not significant for the deep and the shallow beds (AR = 0.6) when pressure dropped to 10^3 Pa from 10^4 Pa. For brevity, the results of shallow beds are shown in the supplementary section.

5. Conclusion

The drag term appearing in the Two-fluid model governing equation was modified in the present work to incorporate the effect of slip flow, which becomes predominant when the fluidised bed is operated at high vacuum pressures, where Kn approaches a value of unity. Two cases were solved numerically: fluidised bed with immersed surface and bubbling fluidisation in shallow and deep beds. Upon comparison with the existing Gidaspow's model, the velocity distributions in the bed were predicted significantly higher by the slip flow drag law, due to which the velocity of solid particles were predicted to be slower than the Gidaspow's model in the fluidised bed with immersed surface. Significant differences were observed in the bubble flow structure and bubble size for bubbling fluidisation in the shallow and the deep beds. In addition, under vacuum conditions, a reversal of flow structure of the emulsion phase was observed and both the drag laws used in the present study predicted it consistently.

Appendix A. Supplementary data

Supplementary data associated with this article can be found, in the online version, at http://dx.doi.org/10.1016/j.apt.2012.04.010.

References

[1] M.A. van der Hoef, M. van Sint Annaland, N.G. Deen, J.A.M. Kuipers, Numerical simulation of dense gas–solid fluidized beds: a multiscale modeling strategy, Annual Review of Fluid Mechanics 40 (2008) 47–70.
[2] J.G. Yates, Effects of temperature and pressure on gas–solid fluidization, Chemical Engineering Science 51 (1996) 167–205.
[3] G.N. Bhat, A.B. Whitehead, Heat transfer in subatmospheric fluidized beds, Australian journal of applied science 14 (1963) 198–203.
[4] S. Kawamura, Y. Suezawa, Mechanism of gas flow in a fluidized bed at low pressure, Kagaku Kogaku 25 (1961) 524.
[5] B. Germain, B. Claudel, Fluidization at mean pressures less than 30 torr, Powder Technology 13 (1976) 115–121.
[6] M.F. Llop, F. Madrid, J. Arnaldos, J. Casal, Fluidization at vacuum conditions. A generalized equation for the prediction of minimum fluidization velocity, Chemical Engineering Science 51 (1996) 5149–5157.
[7] C.Y. Wen, Y.H. Yu, Mechanics of fluidisation, Chemical Engineering Progress Symposium Series 62 (1966) 100.
[8] S. Ergun, Fluid flow through packed columns, Chemical Engineering Progress 48 (1952) 89–94.
[9] J.R. Wank, S.M. George, A.W. Weimer, Vibro-fluidization of fine boron nitride powder at low pressure, Powder Technology 121 (2001) 195–204.
[10] D. Gidaspow, Multiphase Flow and Fluidisation, Academic Press, San Diego, 1994.
[11] M. Syamlal, W. Rogers, T.J. O'Brien, Mfix documentation: Volume I, Theory guide. Technical Report DOE/METC-9411004, NTIS/DE9400087, National Technical Information Service, Springfield, VA, 1993.
[12] S. Chapman, T.G. Cowling, The Mathematical Theory of Non-uniform Gases, second ed., Cambridge University Press, Cambridge, UK, 1961.
[13] A. Srivastava, S. Sundaresan, Analysis of a frictional-kinetic model for gas-particle flow, Powder Technology 129 (2003) 72–85.
[14] D.J. Patil, M. van Sint Annaland, J.A.M. Kuipers, Critical comparison of hydrodynamic models for gas–solid fluidized beds – Part I: bubbling gas-solid fluidized beds operated with a jet, Chemical Engineering Science 60 (2005) 57–72.
[15] P.C. Johnson, R. Jackson, Frictional-collisional constitutive relations for granular materials, with application to plane shearing, Journal of Fluid Mechanics 176 (1987) 67–93.
[16] J.A.M. Kuipers, A Two-fluid Micro Balance Model of Fluidised Bed., in: Twente University, The Netherlands, Enschede, 1990.
[17] D. Kunii, O. Levenspiel, Fluidisation Engineering, 1991.